Applied Catalysis B: Environmental 256 (2019) 117794

Contents lists available at ScienceDirect

Applied Catalysis B: Environmental

journal homepage: www.elsevier.com/locate/apcatb

Photocarving nitrogen vacancies in a polymeric carbon nitride for metal-free oxygen synthesis

Pengju Yang[a,b], Long Wang[a], Hangyu Zhuzhang[a], Ruirui Wang[a], Maria-Magdalena Titirici[c,d], Xinchen Wang[a,*,1]

[a] State Key Laboratory of Photocatalysis on Energy and Environment, College of Chemistry, Fuzhou University, Fuzhou, 350116, China
[b] School of Chemistry and Chemical Engineering, Shanxi University, Taiyuan, 030006, China
[c] School of Engineering and Materials Science, Queen Mary University of London, London, E1 4NS, UK
[d] Department of Chemical Engineering, Imperial College London, South Kensington Campus, SE7 2AZ, London, UK

ARTICLE INFO

Keywords:
Carbon nitride
Nitrogen vacancy
Oxygen production
Photocatalysis

ABSTRACT

Photocatalytic water splitting necessitates robust cocatalysts to accelerate the oxygen evolution reaction (OER). However, most OER cocatalysts are based on noble metal oxides. Besides, the loose interface between semiconductor and cocatalyst results in inefficient charge transfer. The fabrication of photocatalysts with integrated light-harvesting and catalytic centers for OER is therefore desired. Herein, we provide a photocarving strategy to create nitrogen vacancies (NVs) on polymeric carbon nitride (PCN). It is confirmed that the embedded NVs can function as active sites to catalyze OER, while promoting the transfer of the photogenerated charge for OER. As a result, PCN-NVs without any extra noble-metal cocatalyst assistance exhibit an enhanced oxygen evolution rate compared with the pristine PCN. Additionally, the PCN obtained from other precursors can also be engineered by this photocarving method, while promoting oxygen photosynthesis. This work provides an avenue to design light-transducers with combined light-harvesting and catalytic configurations for oxygen synthesis chemistry.

1. Introduction

Photocatalytic water splitting is a promising approach to convert solar energy to fuels [1]. Recently, polymeric carbon nitride (PCN) has attracted much attention in photocatalytic water splitting due to its stability, low-cost, as well as tunable composition and redox potentials. Since 2009, Wang et al. discovered PCN can drive water splitting with visible light, and much advancement has been achieved [2–4]. Nevertheless, the performance of photocatalytic water splitting of PCN remains moderate [5,6]. Water oxidation reaction is a four-electron reaction, which requires the release of electrons and protons from water to produce oxygen [7–9]. Therefore, water oxidation reaction is considered as the determining step in photocatalytic water splitting [8,10,11]. To realize photocatalytic water splitting of PCN on an industrial scale, in principle, it is firstly required to boost oxygen evolution reaction (OER).

Loading a cocatalyst onto a semiconductor is a traditional strategy to promote OER efficiency. [12] Commonly, cocatalysts mainly rely on expensive metals such as Co, Ir and Ru [13–15]. Besides, the structure of the cocatalyst is generally different from that of the photocatalyst [15]. Hence, the interface interaction between cocatalyst and photocatalyst is relatively loose, which seriously influences charge transfer and OER efficiency [1,16]. The surface/interface engineering was usually carried out to ensure an efficient charge transfer [17–21]. This typically requires complicated processes and the promoting effect is unsatisfactory. If a PCN photocatalyst could simultaneously possesse light-harvesting and catalytic functions for OER, it will undoubtedly shorten charge transfer distance [22]. Moreover, the charge transfer resistance could be lowered due to their homogeneous structure [22]. Accordingly, the charge transfer dynamics and the overall reaction efficiency can be greatly promoted. Therefore, the development of unique PCN with bifunctional motifs can achieve high-efficiency oxygen production. Additionally, this conceptual design provides a novel strategy to replace expensive metal cocatalysts, while reducing the system cost.

The surface structures and properties of light-harvesting materials have a significant influence on their efficiency of redox reactions [23]. Some studies have observed that the defects/vacancies within materials can act as active sites to promote their performance. Ye et.al found that the oxygen vacancies in $SrTiO_3$ can lower the activation energy barrier for CO_2 reduction [24]. Zhang's group explored the catalytic

* Corresponding author.
E-mail address: xcwang@fzu.edu.cn (X. Wang).
[1] Http://wanglab.fzu.edu.cn.

https://doi.org/10.1016/j.apcatb.2019.117794
Received 11 April 2019; Received in revised form 26 May 2019; Accepted 29 May 2019
Available online 30 May 2019
0926-3373/

capabilities of oxygen vacancies within BiOBr in the N_2 fixation [25]. It has been proven that anion-vacancy centers are electron deficient [26,27]. Theoretically, water can preferentially adsorb onto the anion-vacancies due to the electron donating nature of water molecule, which can improve the adsorption and dissociation of water and expedite OER kinetics [28–30]. Therefore, anion-defect modulation possibly provides a new avenue to promote the OER performance. Additionally, it is a challenge to manage the defect concentration and their distribution through present methods [31,32]. Hence, the development of innovative procedures for controlled defect design is needed.

Herein, we successfully constructed nitrogen vacancies (NVs) on the PCN surface by a photocarving method. The concentration of NVs can be controlled by regulating light irradiation time. Steady-state photoluminescence (PL), time-resolved PL and transient absorption spectroscopy (TAS) revealed that the NVs can effectively promote the separation and transfer kinetics of the photogenerated charge carriers. Importantly, the electrochemical characterization confirmed that the NVs can function as active sites for OER, promoting the oxygen evolution in PCN. Our developed PCN-NVs without any extra metal cocatalyst assistance exhibited an excellent OER activity.

2. Experimental

2.1. Preparation of PCN and PCN-NVs

Typically, 10 g thiourea (≥99.0%, Sinopharm Chemical Reagent Co., L t d) as precursor was calcined at 550 °C with (5 K/min) and kept at 550 °C for 3 h. The obtained photocatalysts were named PCN. In order to construct NVs on the PCN surface, 0.2 g PCN powder were dispersed into 10 mL aqueous solution (triethanolamine (TEOA, ≥99.0% Sinopharm Chemical Reagent Co., L t d): 1 mL; H_2O: 9 mL) and transfer into a self-made reactor. The TEOA was employed to trap photogenerated holes, thus leaving free photoelectrons to cleave chemical bonds within PCN. The light source was a 300 W Xe lamp (> 420 nm). The system temperature was controlled at 30 °C by a flow of cooling water. After reaction, the samples were washed with pure water and dried in a vacuum oven at 60 °C overnight. The PCN-NVs samples were irradiated for 4 h, 6 h, 8 h, and 10 h were named as PCN-NVs-4, PCN-NVs-6, PCN-NVs-8 and PCN-NVs-10, respectively.

The PCN-U and PCN-M were prepared using urea (≥99.0%, Sinopharm Chemical Reagent Co., L t d), melamine(≥99.0%, Sinopharm Chemical Reagent Co., L t d) as precursor, respectively. The synthesis processes of PCN-U and PCN-M were same to those of the PCN above. Additionally, the preparation processed and conditions of PCN-U-NVs and PCN-M-NVs were also same to those of the PCN-NVs.

2.2. Preparation of CoO_x/PCN

0.2 g PCN was dispersed in 10 mL aqueous solutions containing Co $(NO_3)\cdot 6H_2O$(≥99.0%, Sinopharm Chemical Reagent Co., L t d) and stir for 6 h under room temperature. Then, it was irradiated with LED light (405 nm) for 2 h. Finally, the catalysts were dried in an oven at 60 °C overnight [5].

2.3. Characterization

Scanning electron microscopy (SEM) was investigated on a JSM-7001 F microscope. A Nicolet Magna-IR 550-II spectrometer was performed for fourier transform infrared spectroscopy (FTIR) analysis. The optical absorption was analyzed by a UV–vis-NIR spectrophotometer (Shimadzu UV-3600). Photoluminescence (PL) was measured on a Hitachi F-7000 FL spectrophotometer. X-ray photoelectron spectroscopy (XPS) was carried out to prober the surface composition of samples using a Thermo ESCALAB 250 XPS spectrometer. X-ray powder diffraction pattern was analyzed on a D8 Advance Bruker X-ray diffractometer with Cu *K*α radiation (λ. =0.15406 nm). The specific surface areas of samples were analyzed by a Tristar-3000 apparatus at 77 K. An elemental Analyzer (vario EL CUBE) was used to analyze the overall elemental composition. The time-resolved fluorescence spectra were obtained using a Steady State and Time Resolved Fluorescence Spectrometers (FLSP920). The average lifetime is calculated according to $\tau = \tau_1 \cdot I_1 + \tau_2 \cdot I_2 + \tau_3 \cdot I_3$ (τ_i is the lifetime; I_i is the relative intensity). Transient absorption spectroscopy (TAS) was determined on Edinburgh LP920 specteophotometer with an OPO laser (excitation wavelength: 400 nm). Static water contact angles were conducted using a contact angle goniometer (KSVCM 200) employing drops of pure water at 25 °C. The chemical composition of photocarving processes was analyzed by mass spectrometry (OmniStar).

The N *K*-edge X-ray absorption near-edge spectra (XANES) were obtained at the BL12B-a beamline of National Synchrotron Radiation Laboratory (China) in the total electron yield mode by collecting the sample drain current under a vacuum better than 5×10^{-8} Pa. The beam from the bending magnet was monochromatized utilizing a varied linespacing plane grating and refocused by a toroidal mirror. The energy range is from100 to 1000 eV (energy resolution: 0.2 eV).

Electrochemical measurements were conducted in a chemical cell, using a Pt sheet as the counter electrode, a saturated calomel electrode as the reference electrode and 0.5 M Na_2SO_4 aqueous solution as electrolyte (bias voltage: 0.2 V). The work electrode was prepared by dip-coating sample slurry on ITO glass and then dried under room temperature.

2.4. Photocatalytic tests

The O_2 production reaction was performed in a top-irradiation reactor. 0.01 M $AgNO_3$ and 0.2 g La_2O_3 were employed as electron acceptor and a pH buffer agent, respectively. The 50 mg catalyst was added into 100 mL pure water and stirred well. Then, the system was evacuated to eliminate air before reaction. A 300 W Xe lamp was employed as light source. The O_2 evolution reaction was at controlled 12 °C by a water circulating pump. Gas chromatography was used to analyze O_2 production.

3. Results and discussion

3.1. Synthesis and characterization

The NVs was constructed on the PCN surface by a photocarving method, as illustrated in Fig. 1 (see details in the experimental section). X-ray photoelectron spectroscopy (XPS) was performed to determine the surface configuration of PCN. Table S1 and Fig. 2a present the surface atomic ratios of PCN and PCN after photocarving. Evidently, the surface C/N ratios of PCN regularly increased from 0.852 to 0.902, which indicates that the high-energy photoelectrons can selectively destroy nitrogen-related segments to form NVs. [33] To identify the origin of NVs, C 1s and N 1s spectra (Figures S1-5) were analyzed to quantify the percentages of chemical bonds in PCN. The peaks at 284.6 and 288 ± 0.1 eV from C 1s spectra were assigned to the C═C/C−H and N−C═N bonds, respectively [34]. The peaks at 398.5 ± 0.2, 399.7 ± 0.2 and 401.2 ± 0.2 eV from N 1s spectra were ascribed to the C−N═C, N−$(C)_3$ and C−NH bonds, respectively. [34] Observably, the ratios of C−N═C bonds within PCN gradually decreased after photocarving treatment (Tables S2-3), affirming that the NVs mainly stem from the C−N═C units. The increase ratio of C−H and C−NH bonds (Table S2-S3) along with the hydrogen content (Table S4) suggests that the C−N═C units were principally cut into C−H and C−NH fragments and synchronously a part of N atoms loosed from C−N═C units. Thus, based on the above results and discussion, it is believed that the scission of C−N═C bond principally take place via a hydrogen radical pathway, which is supported by the MS result (Figure S6).

X-ray absorption near-edge spectroscopy (XANES) was used to further identify the chemical configuration of PCN. [35,36] As shown in

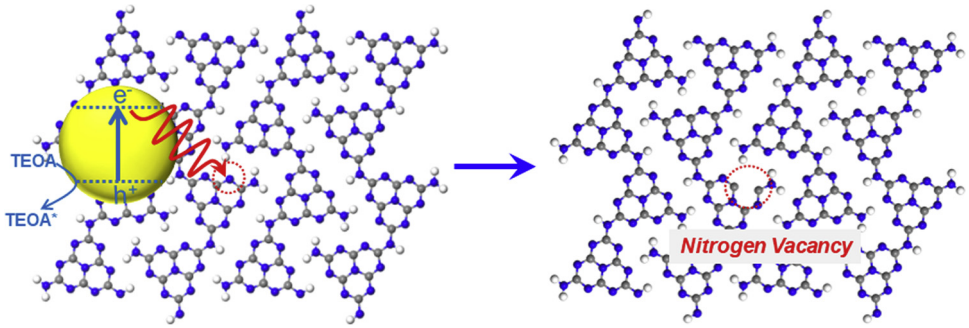

Fig. 1. Illustration of the preparation of PCN-NVs by a photocarving approach.

Fig. 2b, two peaks were observed from nitrogen *K*-edge XANES for PCN and PCN-NVs-6. The peaks at 397 and 400 eV were attributed to C = N−C and central nitrogen, respectively. [35,36] The C=N−C peaks of PCN and PCN-NVs-6 were further compared in the inset of Fig. 2b. The C=N−C peak in PCN-NVs-6 showed a lower intensity compared with pristine PCN. This indicates that the C= N−C bonds within PCN-NVs-6 were partly broken, reaffirming that the NVs stem from the C= N−C units, which is in good agreement with the XPS analysis. [35,36] Elemental analysis (EA) was carried out to determine the bulk C/N ratios of samples. The EA results (Table S4) show that the C/N ratios fluctuate slightly between 0.647 and 0.654. XPS and EA suggest that the NVs were mainly distributed on the PCN surface. Fig. 2c displays the X-ray diffraction (XRD) patterns of samples. The peaks at 27.3° and 13.2° were attributed to the (002) and (100) planes of PCN, respectively. Notably, the peaks of all samples were almost the same, which suggests that the bulk structure of PCN-NVs had no obvious change after photocarving. Nitrogen adsorption-desorption isotherms (Fig. 2d) displays that the nitrogen uptake of PCN was similar to those of PCN-NVs. These results reconfirm that the NVs did not extend into the bulk structure of the PCN.

UV–vis adsorption spectra of the PCN and PCN-NVs are demonstrated in Fig. 3a. The PCN and PCN-NVs showed similar light absorption edges. It is widely accepted that the bulk physicochemical properties of a semiconductor prominently determine its light absorption edge [37]. Thus, the UV/vis result suggests that the bulk physicochemical properties of PCN-NVs were similar to that of the PCN, consistent with the XRD results. The tailed absorption of PCN-NVs in the visible light region is probably related to the introduced NVs [38,39]. Electron paramagnetic resonance (EPR) was performed to further check the formation of NVs. The typical single Lorentzian line (g = 2.0035) was attributed to unpaired electrons in sp^2-carbon atoms within π-conjugated aromatic system. Theoretically, the formation of NVs could donate unpaired electrons to adjacent sp^2-carbon atoms within π-conjugated aromatic rings in PCN. The PCN-NVs showed an enhanced EPR signal compared with pristine PCN (Fig. 3b), which suggests the presence of more unpaired electrons within π-conjugated aromatic rings in PCN-NVs and also manifested the formation of NVs [40,41]. The morphological structures of the PCN and PCN-NVs were characterized by scanning electron microscope (SEM), as shown in Figure S7. The pristine PCN and PCN-NVs exhibited analogous sheet-like structures, in agreement with the XRD and BET results. Fourier Transform Infrared (FTIR) spectra of all samples are presented in Figure S8. The bands at 3000-3500 cm^{-1} suggested the existence of N−H stretching. The bands at 1200-1750 cm^{-1} were attributed to the

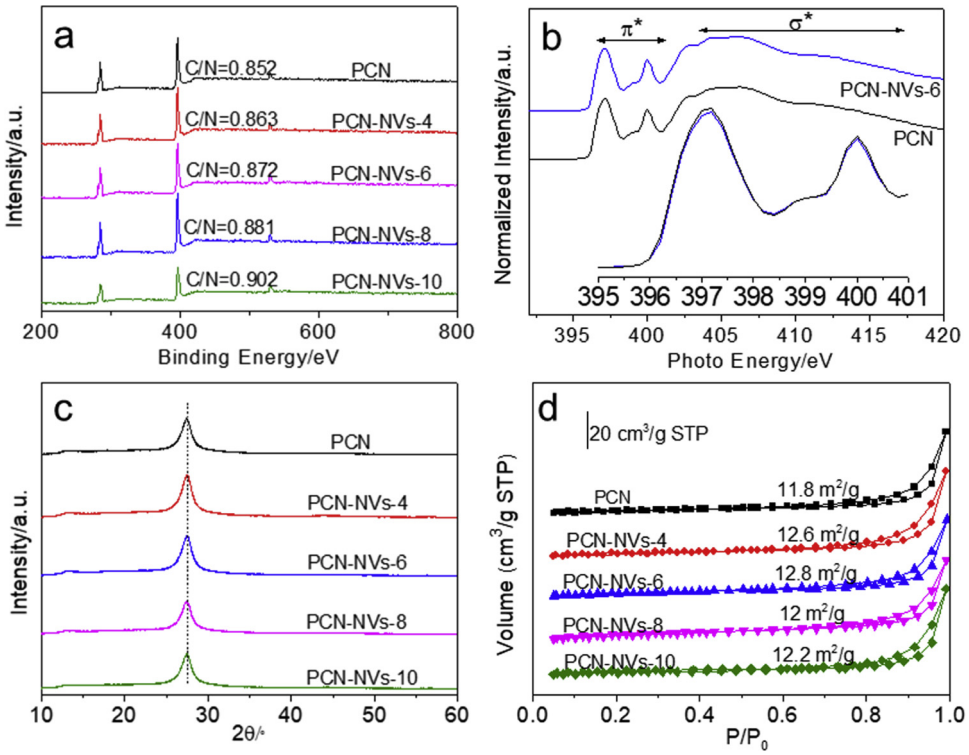

Fig. 2. a) XRD patterns, b) N *K*-edge XANES, c) XRD patterns and d) Nitrogen adsorption-desorption isotherms of PCN and PCN-NVs samples.

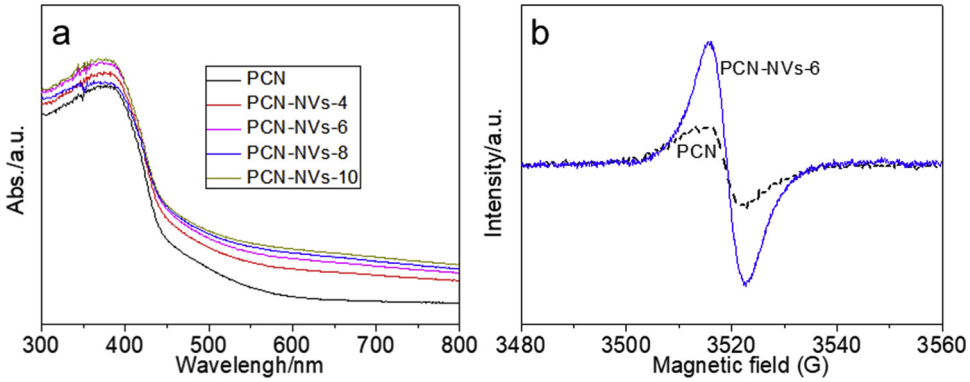

Fig. 3. a) UV–vis adsorption spectra and b) EPR of PCN and PCN-NVs samples.

stretching of CN heterocycles of PCN. The stretching of triazine units was also observed at 810 cm^{-1}. The PCN and PCN-NVs displayed comparable bands, proposing that the basic structure of PCN-NVs was maintained. [42]

The separation and transfer kinetics of the photo-generated charges in PCN and PCN-NVs were studied by steady-state PL, time-resolved PL and TAS spectra. In Figure S9, the PCN-NVs exhibits a weak PL emission compared to pristine PCN. The PL quenching in PCN-NVs could be associated with the NVs [43]. The time-resolved PL results are presented in Fig. 4a and Table S5. The pristine PCN presents a slower nonradiative decay compared with the PCN-NVs-6. The results of steady-state PL and time-resolved PL suggest that the NVs modification can delay the charges recombination of PCN [44,45]. It has been proven that photo-generated holes in PCN can be traced in the visible light region. Therefore, we monitored the TAS signal of the PCN and PCN-NVs at 660 nm to investigate decay processes of holes [44]. Apparently, the decay of holes in PCN-NVs was faster than in PCN (Fig. 4b). The TAS results confirm that the NVs can extract holes, thus accelerating the separation of photogenerated charges and increasing the opportunity of the holes to participate in OER. The transient photocurrent spectra of the PCN and PCN-NVs are shown in Fig. 4c. The PCN-NVs exhibited a greater photocurrent than the PCN under identical conditions. The semicircular radius in the impedance spectra of PCN-NVs-6 was obviously smaller than that of pristine PCN, suggesting an efficient interfacial charge transport resistance (Fig. 4d). Thus, the results of photocurrent and impedance spectra indicate that the NVs could facilitate the interfacial charge transfer and separation, thus increasing the chance of photogenerated charge carriers for participating redox catalysis. The conduction band (CB) and valance band (VB) positions of PCN and PCN-NVs-6 were analyzed by Mott-Schottky plots and Tauc plots, as shown in Figures S10-11. The VB value of PCN-NVs-6 were slightly larger than that of PCN. This suggests a stronger driving force of PCN-NVs-6 for water oxygen and thus partly accounted for its enhanced oxygen evolution performance.

To explore the catalytic function of the NVs, electrochemical experiments are implemented. Fig. 5a recorded the liner sweep voltammetry (LSV) curves of the PCN and PCN-NVs at a scan rate of 10 mV s^{-1}. Impressively, the PCN had a large overpotential for water oxidation, whereas a reduced overpotential and an enhanced current density were observed when the PCN was engineered by the NVs. This observation suggests that the NVs can function as active sites to catalyze the water oxidation reaction [46,47]. The current density of PCN and

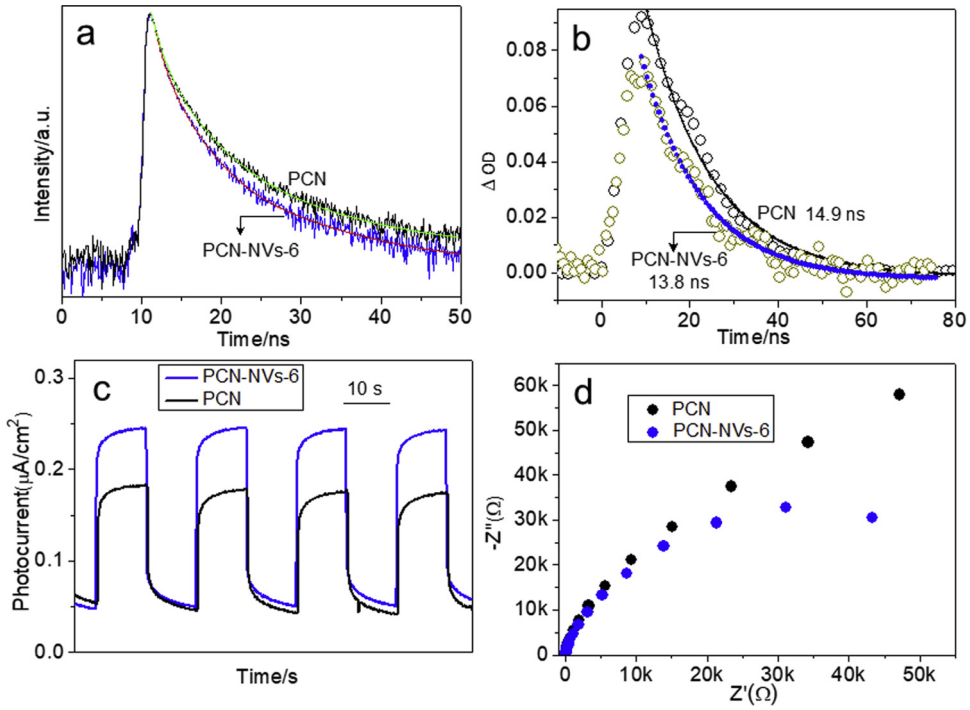

Fig. 4. a) Time-resolved PL, b) TAS, c) Transient photocurrent and d) electrochemical impedance results of PCN and PCN-NVs-6.

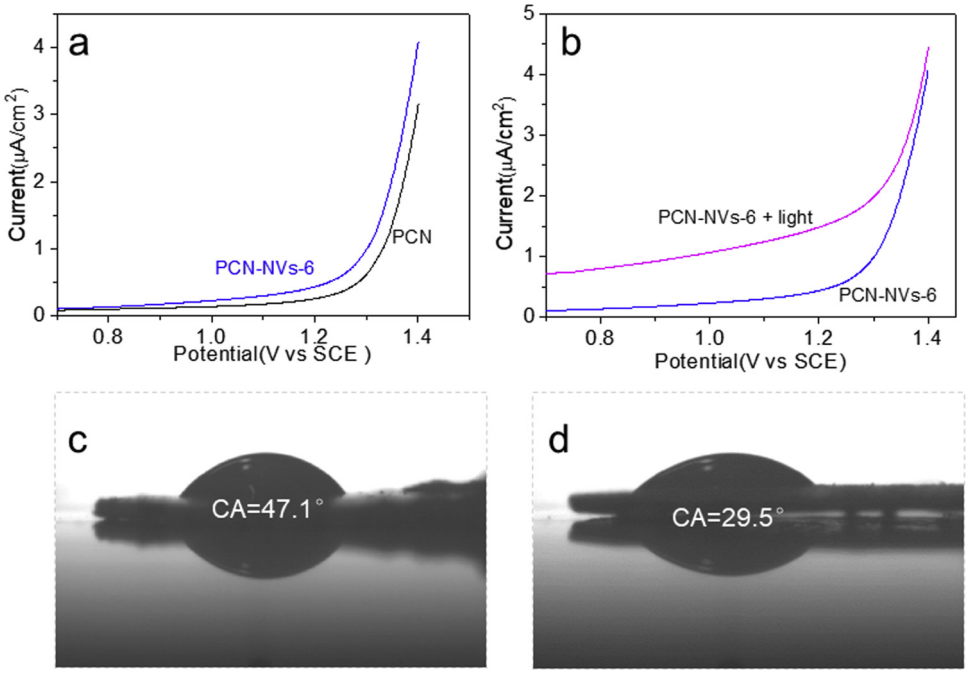

Fig. 5. a) LSV curves of PCN and PCN-NVs-6, b) LSV curves of PCN-NVs-6 under dark and visible light, CA measurement of c) PCN and d) PCN-NVs-6.

PCN-NVs catalysts for water oxidation can be further increased upon the visible light irradiation. Besides, the potential was shifted to the negative direction (Figs. 5b and S12). These findings illustrates that the light energy can strengthen the water oxidation reaction, consistent with the previous report [48]. Contact angle (CA) experiments are displayed in Fig. 5c-d. The PCN-NVs presented a CA of 29.5° compared with 47.1° for PCN. Previous literatures proposed that defect sites can facilitate water adsorption and dissociation due to the electron donating feature of water molecule [30,49]. Zhao and coworker also found that the defects within PCN played a key role in the adsorption and dissociation of water by theory calculations [50]. Hence, it was reasonable to assume that the NVs prefer to adsorb water molecules enabling the PCN-NVs with a more hydrophilic surface. The improved hydrophilicity lowered the activation energy for water diffusion and dissociation because the water was more attracted to the surface and nearby surface water, which advanced water adsorption and subsequent water oxidation.

3.2. Photocatalytic oxygen production

The photocatalytic oxygen production was investigated to explore the effects of NVs on water oxidation reaction. Fig. 6a exhibits the photocatalytic oxygen evolution rates of PCN and PCN-NVs samples under a 300 W Xe lamp irradiation. Noticeably, the pristine PCN showed low activity for oxygen production, whereas the oxygen production rates of PCN-NVs samples were enhanced obviously. The optimized oxygen production rate of PCN-NVs was 4.2 time higher than that of the pristine PCN, suggesting that the defect engineering was a capable approach to improve OER efficiency. Fig. 6b shows the oxygen evolution from PCN and PCN-NVs catalysts in a 4 -h reaction. The oxygen evolution rates displayed a slowdown trend for all the catalysts. This probably related to the formed Ag nanoparticles due to Ag^+ reduction, which hindered the optical adsorption of PCN and blocked active sites for oxygen evolution. The results of PL, time-resolved PL, LSV and CA suggest that the NVs demonstrated multifunctional characters. On the one hand, it can capture the photogenerated holes and prohibit the charge recombination of PCN. On the other hand, the NVs can function as catalytical sites to lower the reaction barrier for OER. The synergistic effects advanced the sluggish kinetic of OER, thus helping the oxygen production. The proposed mechanism is shown in Fig. 6c. We also prepared CoO_x/PCN and studied its photocatalytic performance. When the CoO_x was loaded over the PCN as an OER co-catalyst, the oxygen production rate of CoO_x/PCN was increased to 4.8 μmol h^{-1} (Figure S13). Evidently, the promote effect of the CoO_x cocatalyst was moderate. This indicates that the in-situ assembly of functionalized defects within PCN skeleton was feasible to promote redox catalysis.

To show the generality of photocarving approach, PCN synthesized from urea and melamine precursors were also engineered by this method. The XRD results of PCN-U and PCN-M samples are shown in Fig. 7a and b. The peaks intensity and position of all samples were almost the same, indicating that the structure was retained. The XPS results confirmed that the NVs were introduced on the surface of PCN-U and PCN-M (Figures S14-15; Tables S6-9), consistent with the EPR results (Fig. 7c and d). The tailed absorption in the visible light region of PCN-U-NVs and PCN-M-NVs (Figure S16) was attributed to the formed NVs. The BET, FTIR and SEM results of PCN-U, PCN-M, PCN-U-NVs and PCN-M-NVs are given in Figures S17-19, respectively. The PL spectra of the PCN-U, PCN-M, PCN-U-NVs and PCN-M-NVs are shown in Figure S20. The PL emission intensities of the PCN-U-NVs and PCN-M-NVs samples were lowered, implying a decreased recombination of photogenerated charges [51]. The photocatalytic performance and stability of the PCN-U, PCN-M, PCN-U-NVs and PCN-M-NVs are presented in Fig. 8. Expectedly, the PCN-U-NVs and PCN-M-NVs samples demonstrated an enhanced oxygen production activity, reconfirming the viability and effectiveness of defect modulation for OER.

4. Conclusion

In summary, we demonstrated a novel photocarving method to construct NVs on the PCN surface. The PL, time-resolved PL, TAS and electrochemical results confirmed that the NVs can function as active sites for OER, while preventing recombination of the photogenerated charges, thereby boosting OER performance. The results showed that the oxygen evolution rate of the PCN-NVs without extra noble-metal cocatalysts assistance was higher than that of the PCN. This work not only provides an innovative approach to design defects within PCN matrix, but also open up new opportunities for the fabrication of

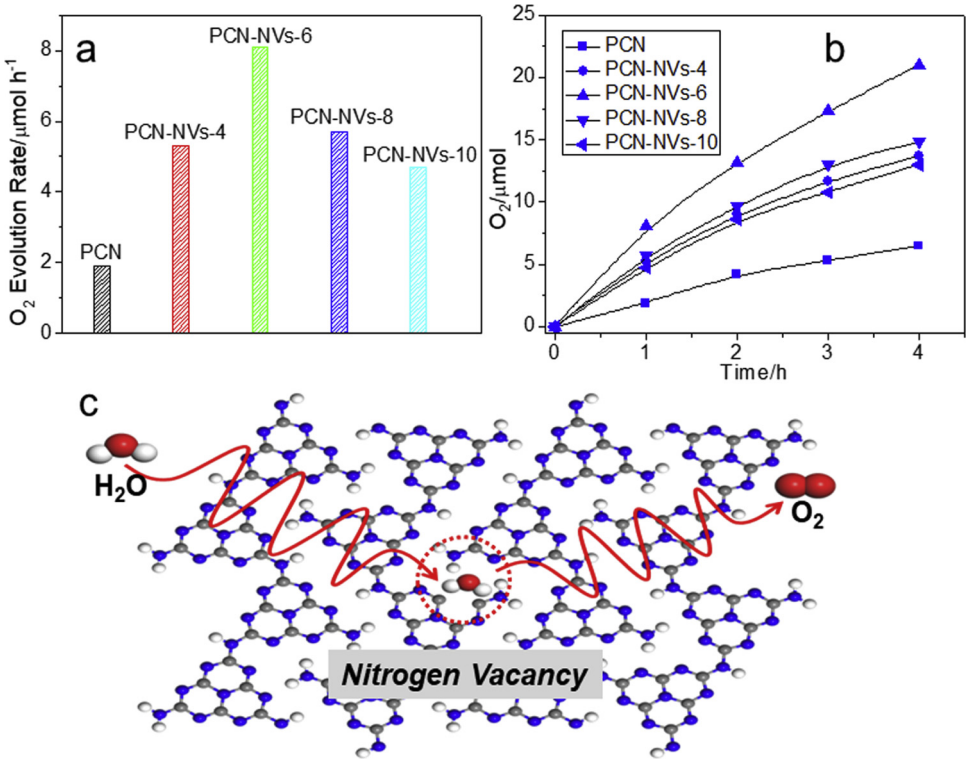

Fig. 6. a) Photocatalytic O_2 evolution rates over PCN and PCN-NVs samples (50 mg photocatalyst, 300 W Xe lamp, 285 K), b) The generated O_2 as a function of irradiation time(50 mg photocatalyst, 300 W Xe lamp, 285 K) and c) The proposed mechanism for photocatalytic O_2 production.

exceptional 2D light-transducers for metal-free oxygen photosynthesis.

Notes

The authors declare no competing financial interest.

Acknowledgments

This work was financially supported by the National Natural Science Foundation of China (21761132002, 21425309, 21703039, and 21861130353), the National Key R&D Program of China

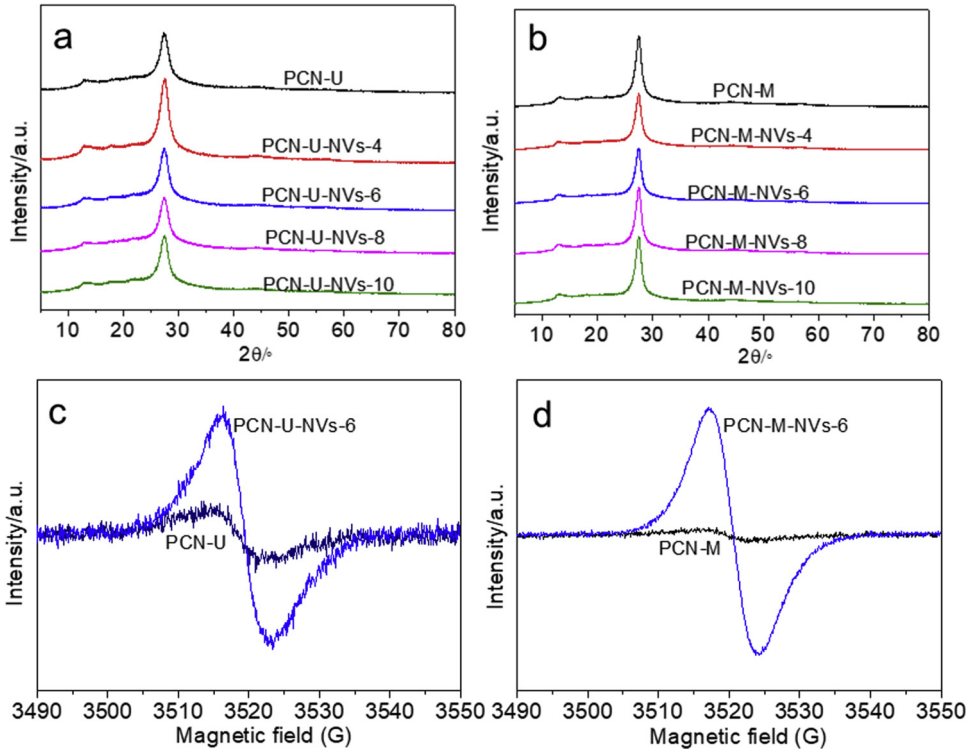

Fig. 7. XRD patterns of PCN-U(a) and PCN-M (b) samples, EPR results of PCN-U (c) and PCN-M (d).

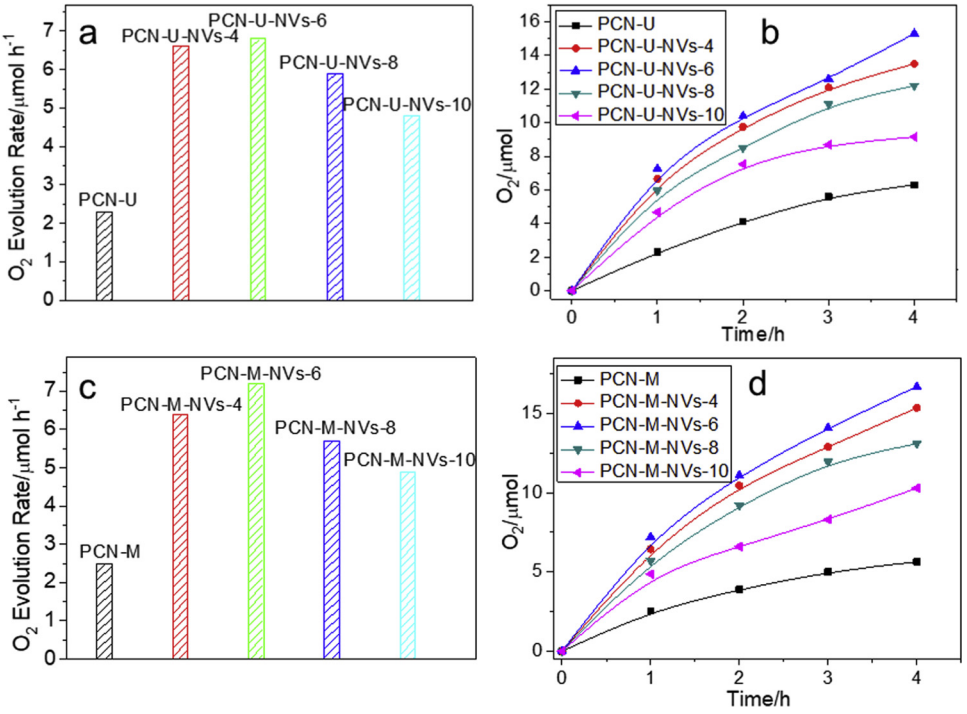

Fig. 8. Photocatalytic O_2 evolution rates (a) and the generated O_2 as a function of irradiation time (b) of PCN-U-based samples (50 mg photocatalyst, 300 W Xe lamp, 285 K); Photocatalytic O_2 evolution rates (c) and the generated O_2 as a function of irradiation time (d) of PCN-M-based samples (50 mg photocatalyst, 300 W Xe lamp, 285 K).

(2018YFA0209301), the National Basic Research Program of China (2013CB632405), the Chang Jiang Scholars Program of China (T2016147) and the 111 Project (D16008). We also thank the National Synchrotron Radiation Laboratory of China for providing the beam time from station BL12B-a measurements. Xinchen Wang would like to thank the Royal Society for an Advanced Newton Fellowship (NAF \R1\180198) to enable the collaboration with Prof. Titirici.

Appendix A. Supplementary data

Supplementary material related to this article can be found, in the online version, at doi:https://doi.org/10.1016/j.apcatb.2019.117794.

References

[1] S. Chen, T. Takata, K. Domen, Particulate photocatalysts for overall water splitting, Nat. Rev. Mater. 2 (2017) 17050.
[2] X.C. Wang, K. Maeda, A. Thomas, K. Takanabe, G. Xin, J.M. Carlsson, K. Domen, M. Antonietti, A metal-free polymeric photocatalyst for hydrogen production from water under visible light, Nat. Mater. 8 (2009) 76–80.
[3] J. Sun, J. Zhang, M. Zhang, M. Antonietti, X. Fu, X. Wang, Bioinspired hollow semiconductor nanospheres as photosynthetic nanoparticles, Nat. Commun. 3 (2012) 1139.
[4] X.C. Wang, X.F. Chen, A. Thomas, X.Z. Fu, M. Antonietti, Metal-containing carbon nitride compounds: a new functional organic-metal hybrid material, Adv. Mater. 21 (2009) 1609–1612.
[5] G. Zhang, Z.-A. Lan, L. Lin, S. Lin, X. Wang, Overall water splitting by Pt/g-C_3N_4 photocatalysts without using sacrificial agents, Chem. Sci. 7 (2016) 3062–3066.
[6] D. Zheng, X.-N. Cao, X. Wang, Precise formation of a hollow carbon nitride structure with a Janus surface to promote water splitting by photoredox catalysis, Angew. Chem.Int. Edit. 55 (2016) 11512–11516.
[7] G. Zhang, C. Huang, X. Wang, Dispersing molecular cobalt in graphitic carbon nitride frameworks for photocatalytic water oxidation, Small 11 (2015) 1215–1221.
[8] G. Zhang, S. Zang, X. Wang, Layered $Co(OH)_2$ deposited polymeric carbon nitrides for photocatalytic water oxidation, ACS Cata. 5 (2015) 941–947.
[9] J.-X. Li, C. Ye, X.-B. Li, Z.-J. Li, X.-W. Gao, B. Chen, C.-H. Tung, L.-Z. Wu, A redox shuttle accelerates O_2 evolution of photocatalysts formed in situ under visible light, Adv. Mater. 29 (2017) 1606009.
[10] M.D. Karkas, E.V. Johnston, O. Verho, B. Akermark, Artificial photosynthesis: photosynthesis: from nanosecond electron transfer to catalytic water oxidation, Acc. Chem. Res. 47 (2014) 100–111.
[11] H. Li, J. Shang, H. Zhu, Z. Yang, Z. Ai, L. Zhang, Oxygen vacancy structure associated photocatalytic water oxidation of BiOCl, ACS Cata. 6 (2016) 8276–8285.
[12] W. Ruttinger, G.C. Dismukes, Synthetic water-oxidation catalysts for artificial photosynthetic water oxidation, Chem. Rev. 97 (1997) 1–24.
[13] V. Petrykin, K. Macounova, O.A. Shlyakhtin, P. Krtil, Tailoring the selectivity for electrocatalytic oxygen evolution on ruthenium oxides by zinc substitution, Angew. Chemie Int. Ed. English 49 (2010) 4813–4815.
[14] T. Hisatomi, J. Kubota, K. Domen, Recent advances in semiconductors for photocatalytic and photoelectrochemical water splitting, Chem. Soc. Rev. 43 (2014) 7520–7535.
[15] J. Yang, D. Wang, H. Han, C. Li, Roles of cocatalysts in photocatalysis and photoelectrocatalysis, Acc. Chem. Res. 46 (2013) 1900–1909.
[16] K. Domen, Development of H_2 evolution sites for overall water splitting on particulate photocatalysts, Abstr. Pap. Am. Chem. Soc. 233 (2007) 204.
[17] S. Chen, S. Shen, G. Liu, Y. Qi, F. Zhang, C. Li, Interface engineering of a CoO_x/Ta_3N_5 photocatalyst for unprecedented water oxidation performance under visible-light-irradiation, Angew. Chemie Int. Ed. English 54 (2015) 3047–3051.
[18] G.G. Zhang, Z.A. Lan, X.C. Wang, Surface engineering of graphitic carbon nitride polymers with cocatalysts for photocatalytic overall water splitting, Chem. Sci. 8 (2017) 5261–5274.
[19] Q. Xiang, J. Yu, M. Jaroniec, Synergetic effect of MoS_2 and graphene as cocatalysts for enhanced photocatalytic H_2 production activity of TiO_2 nanoparticles, J. Am. Chem. Soc. 134 (2012) 6575–6578.
[20] Y. Lei, H. Jia, W. He, Y. Zhang, L. Mi, H. Hou, G. Zhu, Z. Zheng, Hybrid solar cells with outstanding short-circuit currents based on a room temperature soft-chemical strategy: the case of P_3HT:Ag_2S, J. Am. Chem. Soc. 134 (2012) 17392–17395.
[21] R. Liu, Z. Zheng, J. Spurgeon, X. Yang, Enhanced photoelectrochemical water-splitting performance of semiconductors by surface passivation layers, Energy Environ. Sci. 7 (2014) 2504–2517.
[22] J. Ran, J. Zhang, J. Yu, M. Jaroniec, S.Z. Qiao, Earth-abundant cocatalysts for semiconductor-based photocatalytic water splitting, Chem. Soc. Rev. 43 (2014) 7787–7812.
[23] A.L. Linsebigler, G.Q. Lu, J.T. Yates, Photocatalysis on TIO2 surfaces - principles, mechanisms, and selected results, Chem. Rev. 95 (1995) 735–758.
[24] K. Xie, N. Umezawa, N. Zhang, P. Reunchan, Y.J. Zhang, J.H. Ye, Self-doped $SrTiO_3$-delta photocatalyst with enhanced activity for artificial photosynthesis under visible light, Energy Environ. Sci. 4 (2011) 4211–4219.
[25] H. Li, J. Shang, Z. Ai, L. Zhang, Efficient visible light nitrogen fixation with BiOBr nanosheets of oxygen vacancies on the exposed {001} facets, J. Am. Chem. Soc. 137 (2015) 6393–6399.
[26] Z.Y. Lu, C.J. Nicklaw, D.M. Fleetwood, R.D. Schrimpf, S.T. Pantelides, Structure, properties, and dynamics of oxygen vacancies in amorphous SiO_2, Phys. Rev. Lett. 89 (2002) 4.
[27] T. Hashizume, R. Nakasaki, Discrete surface state related to nitrogen-vacancy defect on plasma-treated GaN surfaces, Appl. Phys. Lett. 80 (2002) 4564–4566.
[28] M. Mifsud, S. Gargiulo, S. Iborra, I.W.C.E. Arends, F. Hollmann, A. Corma, Photobiocatalytic chemistry of oxidoreductases using water as the electron donor, Nat. Commun. 5 (2014) 3145.
[29] A.J. Bard, M.A. Fox, Artificial photosynthesis - solar splitting of water to hydrogen and oxygen, Acc. Chem. Res. 28 (1995) 141–145.
[30] O. Bikondoa, C.L. Pang, R. Ithnin, C.A. Muryn, H. Onishi, G. Thornton, Direct visualization of defect-mediated dissociation of water on TiO_2 (110), Nat. Mater. 5 (2006) 189–192.
[31] L. Schmidt-Mende, J.L. MacManus-Driscoll, ZnO nanostructures, defects, and devices, Mater. Today 10 (2007) 40–48.

[32] M.V. Ganduglia-Pirovano, A. Hofmann, J. Sauer, Oxygen vacancies in transition metal and rare earth oxides: current state of understanding and remaining challenges, Surf. Sci. Rep. 62 (2007) 219–270.
[33] P. Yang, H. Ou, Y. Fang, X. Wang, A facile steam reforming strategy to delaminate layered carbon nitride semiconductors for photoredox catalysis, Angew. Chemie Int. Ed. English 56 (2017) 3992–3996.
[34] Y. Zheng, L. Lin, B. Wang, X. Wang, Graphitic carbon nitride polymers toward sustainable photoredox catalysis, Angew. Chemie Int. Ed. English 54 (2015) 12868–12884.
[35] Y. Zheng, Y. Jiao, Y.H. Zhu, L.H. Li, Y. Han, Y. Chen, A.J. Du, M. Jaroniec, S.Z. Qiao, Hydrogen evolution by a metal-free electrocatalyst, Nat. Commun. 5 (2014) 8.
[36] S.C. Ray, C.W. Pao, J.W. Chiou, H.M. Tsai, J.C. Jan, W.F. Pong, R. McCann, S.S. Roy, P. Papakonstantinou, J.A. McLaughlin, Electronic properties of a-CN_x thin films: an x-ray-absorption and photoemission spectroscopy study, J. Appl. Phys. 98 (2005) 033708.
[37] A.M. Smith, S. Nie, Semiconductor nanocrystals: structure, properties, and band gap engineering, Acc. Chem. Res. 43 (2010) 190–200.
[38] H.J. Yu, R. Shi, Y.X. Zhao, T. Bian, Y.F. Zhao, C. Zhou, G.I.N. Waterhouse, L.Z. Wu, C.H. Tung, T.R. Zhang, Alkali-assisted synthesis of nitrogen deficient graphitic carbon nitride with tunable band structures for efficient visible-light-Driven hydrogen evolution, Adv. Mater. 29 (2017) 8.
[39] P. Niu, L.-C. Yin, Y.-Q. Yang, G. Liu, H.-M. Cheng, Increasing the visible light absorption of graphitic carbon nitride (Melon) photocatalysts by homogeneous self-modification with nitrogen vacancies, Adv. Mater. 26 (2014) 8046–8052.
[40] Y. Zhao, Y. Zhao, G.I.N. Waterhouse, L. Zheng, X. Cao, F. Teng, L.-Z. Wu, C.-H. Tung, D. O'Hare, T. Zhang, Layered-double-Hydroxide nanosheets as efficient visible-light-driven photocatalysts for dinitrogen fixation, Adv. Mater. 29 (2017) 1703828.
[41] H. Kaftelen, K. Ocakoglu, R. Thomann, S. Tu, S. Weber, E. Erdem, EPR and photoluminescence spectroscopy studies on the defect structure of ZnO nanocrystals, Phys. Rev. B 86 (2012).
[42] W.J. Ong, L.L. Tan, Y.H. Ng, S.T. Yong, S.P. Chai, Graphitic carbon nitride (g-C_3N_4)-Based photocatalysts for artificial photosynthesis and environmental remediation: are we a step closer to achieving sustainability? Chem. Rev. 116 (2016) 7159–7329.
[43] G. Zhao, G. Liu, H. Pang, H. Liu, H. Zhang, K. Chang, X. Meng, X. Wang, J. Ye, Improved photocatalytic H_2 evolution over G-carbon nitride with enhanced in-plane ordering, Small 12 (2016) 6160–6166.
[44] C. Ye, X.Z. Wang, J.X. Li, Z.J. Li, X.B. Li, L.P. Zhang, B. Chen, C.H. Tung, L.Z. Wu, Protonated graphitic carbon nitride with surface attached molecule as hole relay for efficient photocatalytic O_2 evolution, ACS Cata. 6 (2016) 8336–8341.
[45] K.L. Corps, C.W. Schlenker, Ultrafast spectroscopy reveals electron-transfer cascade that improves hydrogen evolution with carbon nitride photocatalysts, J. Am. Chem. Soc. 139 (2017) 7904–7912.
[46] M. Zhong, T. Hisatomi, Y. Kuang, J. Zhao, M. Liu, A. Iwase, Q. Jia, H. Nishiyama, T. Minegishi, M. Nakabayashi, N. Shibata, R. Niishiro, C. Katayama, H. Shibano, M. Katayama, A. Kudo, T. Yamada, K. Domen, Surface modification of CoO_x loaded $BiVO_4$ photoanodes with ultrathin p-Type NiO layers for improved solar water oxidation, J. Am. Chem. Soc. 137 (2015) 5053–5060.
[47] F. Zhang, A. Yamakata, K. Maeda, Y. Moriya, T. Takata, J. Kubota, K. Teshima, S. Oishi, K. Domen, Cobalt-modified porous single-crystalline $LaTiO_2N$ for highly efficient water oxidation under visible light, J. Am. Chem. Soc. 134 (2012) 8348–8351.
[48] G. Liu, P. Li, G. Zhao, X. Wang, J. Kong, H. Liu, H. Zhang, K. Chang, X. Meng, T. Kako, J. Ye, Promoting active species generation by plasmon-induced hot-electron excitation for efficient electrocatalytic oxygen evolution, J. Am. Chem. Soc. 138 (2016) 9128–9136.
[49] M.K. Kostov, E.E. Santiso, A.M. George, K.E. Gubbins, M.B. Nardelli, Dissociation of water on defective carbon substrates, Phys. Rev. Lett. 95 (2005) 4.
[50] H.-Z. Wu, L.-M. Liu, S.-J. Zhao, The role of the defect on the adsorption and dissociation of water on graphitic carbon nitride, Appl. Surf. Sci. 358 (2015) 363–369.
[51] L.Q. Jing, Y.C. Qu, B.Q. Wang, S.D. Li, B.J. Jiang, L.B. Yang, W. Fu, H.G. Fu, J.Z. Sun, Review of photoluminescence performance of nano-sized semiconductor materials and its relationships with photocatalytic activity, Sol. Energy Mater. Sol. Cells 90 (2006) 1773–1787.